



## Strengthening and softening in gradient nanotwinned FCC metallic multilayers

Yuanyuan Tian(田圆圆), Gangjie Luo(罗港杰), Qihong Fang(方棋洪), Jia Li(李甲), and Jing Peng(彭静)

**Citation:** Chin. Phys. B, 2022, 31 (6): 066204. DOI: 10.1088/1674-1056/ac4cc6

Journal homepage: <http://cpb.iphy.ac.cn>; <http://iopscience.iop.org/cpb>

### What follows is a list of articles you may be interested in

---

## Effect of void size and Mg contents on plastic deformation behaviors of Al-Mg alloy with pre-existing void: Molecular dynamics study

Ning Wei(魏宁), Ai-Qiang Shi(史爱强), Zhi-Hui Li(李志辉), Bing-Xian Ou(区炳显), Si-Han Zhao(赵思涵), and Jun-Hua Zhao(赵军华)

Chin. Phys. B, 2022, 31 (6): 066203. DOI: 10.1088/1674-1056/ac4a74

## Molecular dynamics study of coupled layer thickness and strain rate effect on tensile behaviors of Ti/Ni multilayered nanowires

Meng-Jia Su(宿梦嘉), Qiong Deng(邓琼), Lan-Ting Liu(刘兰亭), Lian-Yang Chen(陈连阳), Meng-Long Su(宿梦龙), and Min-Rong An(安敏荣)

Chin. Phys. B, 2021, 30 (9): 096201. DOI: 10.1088/1674-1056/abf10a

## Plastic deformation mechanism transition of Ti/Ni nanolaminate with pre-existing crack: Molecular dynamics study

Meng-Jia Su(宿梦嘉), Qiong Deng(邓琼)†, Min-Rong An(安敏荣), and Lan-Ting Liu(刘兰亭)

Chin. Phys. B, 2020, 29 (11): 116201. DOI: 10.1088/1674-1056/aba2e5

## Balancing strength and plasticity of dual-phase amorphous/crystalline nanostructured Mg alloys

Jia-Yi Wang(王佳怡), Hai-Yang Song(宋海洋), Min-Rong An(安敏荣), Qiong Deng(邓琼), Yu-Long Li(李玉龙)

Chin. Phys. B, 2020, 29 (6): 066201. DOI: 10.1088/1674-1056/ab84d5

## Anisotropic plasticity of nanocrystalline Ti: A molecular dynamics simulation

Minrong An(安敏荣), Mengjia Su(宿梦嘉), Qiong Deng(邓琼), Haiyang Song(宋海洋), Chen Wang(王晨), Yu Shang(尚玉)

Chin. Phys. B, 2020, 29 (4): 046201. DOI: 10.1088/1674-1056/ab7188

---

# Strengthening and softening in gradient nanotwinned FCC metallic multilayers

Yuanyuan Tian(田圆圆), Gangjie Luo(罗港杰), Qihong Fang(方棋洪)<sup>†</sup>,  
Jia Li(李甲)<sup>‡</sup>, and Jing Peng(彭静)

State Key Laboratory of Advanced Design and Manufacturing for Vehicle Body, Hunan University, Changsha 410082, China

(Received 9 October 2021; revised manuscript received 21 December 2021; accepted manuscript online 19 January 2022)

Plastic-deformation behaviors of gradient nanotwinned (GNT) metallic multilayers are investigated in nanoscale via molecular dynamics simulation. The evolution law of deformation behaviors of GNT metallic multilayers with different stacking fault energies (SFEs) during nanoindentation is revealed. The deformation behavior transforms from the dislocation dynamics to the twinning/detwinning in the GNT Ag, Cu, to Al with SFE increasing. In addition, it is found that the GNT Ag and GNT Cu strengthen in the case of a larger twin gradient based on more significant twin boundary (TB) strengthening and dislocation strengthening, while the GNT Al softens due to more TB migration and dislocation nucleation from TB at a larger twin gradient. The softening mechanism is further analyzed theoretically. These results not only provide an atomic insight into the plastic-deformation behaviors of certain GNT metallic multilayers with different SFEs, but also give a guideline to design the GNT metallic multilayers with required mechanical properties.

**Keywords:** plastic deformation, gradient nanotwinned metallic multilayers, nanoindentation, molecular dynamics simulation

**PACS:** 62.20.F-, 61.72.Mm, 68.35.bd, 02.70.Ns

**DOI:** 10.1088/1674-1056/ac4cc6

## 1. Introduction

Twin boundaries (TBs), as a kind of low energy symmetric grain boundary, has been experimentally found to be effective in changing material properties. In particular, TBs can efficiently improve strength and toughness of many materials without trade-off.<sup>[1,2]</sup> Therefore, nanotwinned (NT) materials with TB structures possess great development potential and application prospect. Lots of works have been carried out to study effects of TBs on mechanical properties of materials. For example, the plastic deformation mechanism of NT Cu is thoroughly analyzed by *in situ* nanoindentation experiment and atomic simulation.<sup>[3]</sup> The result reveals that in addition to acting as barriers to slip transmission, TBs can react with lattice dislocations to facilitate the multiplication of partial dislocations, resulting in the TB translation. During the deformation of NT Al, TBs can effectively resist the dislocation blockage and cause work hardening.<sup>[4]</sup> TBs can simultaneously play hardening and softening roles when the NT diamond is subjected to nanoindentation.<sup>[5]</sup>

In addition, gradient hierarchical materials have appeared with tunable microstructure distribution.<sup>[6,7]</sup> The strain gradient evades the trade-off of strength and ductility. Thus, appropriate introduction of gradient structure into metallic materials can significantly improve mechanical properties of materials. These studies mainly focus on the effect of gradient structure on the mechanical properties of materials in comparison to non-gradient structure. Based on the above consideration, the gradient nanotwinned (GNT) metallic multilayer

structure is proposed in this work. Two types of nanotwinned (GNT) metallic multilayers with different gradient degrees are constructed to investigate the effect of gradient degree on the mechanical properties and deformation behaviors.

Molecular dynamics (MD) simulation, as a powerful means, has been widely used to study the effect of TBs on the deformation behaviors of metal materials.<sup>[8-12]</sup> For example, the uniaxial tension of NT Cu/Ag multilayers is conducted through MD simulation.<sup>[10]</sup> The result quantitatively reveals the effect of twin thickness on the strength. Based on MD simulation, the effects of TBs on the deformation mechanism of NT Ta is uncovered.<sup>[11]</sup> The softening mechanism dominates the deformation of NT Ta with small twin thickness during nanoindentation.<sup>[11]</sup> In addition, it is observed through MD simulation that TBs in the NT TiN films with large twin thickness contribute to the material hardening under nanoindentation.<sup>[12]</sup> The above-mentioned studies fully indicate that MD simulation method plays an important role in deep understanding the effect of TB on the deformation mechanisms and mechanical properties of materials.

Hence, we employ the MD simulation method to investigate the plastic deformations of certain GNT metallic multilayers. The GNT metallic multilayers of Al, Cu, and Ag (GNT Al, GNT Cu, and GNT Ag) are selected as study objects, to reveal the plastic-deformation behaviors of the GNT metallic multilayers with different stacking fault energies (SFEs) during nanoindentation. Here, the SFEs of GNT Al, Cu, and Ag (148 mJ/m<sup>2</sup>, 46 mJ/m<sup>2</sup> and 15 mJ/m<sup>2</sup>) calculated in the current MD simulations belong to high, medium, and low SFE

<sup>†</sup>Corresponding author. E-mail: fangqh1327@hnu.edu.cn

<sup>‡</sup>Corresponding author. E-mail: lijia123@hnu.edu.cn

magnitudes, respectively, and are obviously closed to the experiment values.<sup>[13,14]</sup> This also demonstrates the reliability of our simulation results.

## 2. Simulation models and methods

The MD-simulation model includes the indenter and the substrates of GNT Al, Cu, and Ag (Fig. 1). The spherical diamond indenter with radius of 4 nm is treated as rigid body because of its stiffness.<sup>[4]</sup> The size of substrates is  $20 \times 20 \times 15 \text{ nm}^3$ . Although the size of indenter is at least 100 nm in the nanoindentation experiment, the size of indenter must be small during the nanoindentation of MD simulation due to the computational cost. Referring to the previous MD work,<sup>[15–19]</sup> the radius of indenter is usually set to 26 nm. Here, the indenter radius of 4 nm is selected in our simulation. In addition,

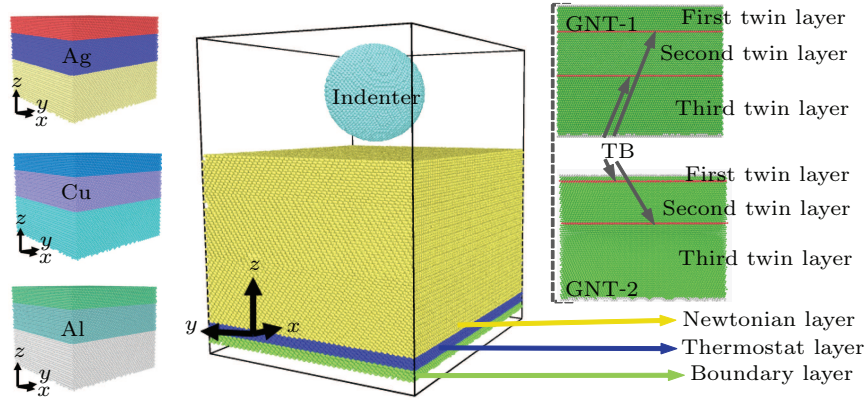


**Fig. 1.** MD models of GNT Al, Cu, and Ag under nanoindentation. Three twin lamellas with different thicknesses are colored with three colors in GNT Al, Cu, and Ag, respectively. Newtonian, thermostat, and boundary layers are colored by different colors and indicated by corresponding arrows.

The crystal orientations of substrates,  $[\bar{1}10]$ ,  $[\bar{1}\bar{1}2]$ , and  $[111]$ , are assigned to  $x$ ,  $y$ , and  $z$  axes. The  $(111)$  surface of substrates is indented along  $[\bar{1}\bar{1}\bar{1}]$  direction. Periodic boundary conditions are maintained in  $x$  and  $y$  directions.<sup>[22–24]</sup> The substrates include the boundary, thermostat, and Newtonian layers (Fig. 1). The boundary layer is fixed to avoid substrate movement. The thermostat layer is kept at 293 K to simulate heat dissipation. The thermostat and Newtonian layers obey Newton's second law.<sup>[23,25]</sup> The velocities of thermostat atoms are rescaled at every 10 computation time steps via the velocity rescaling method when the temperature departs more than 1 K at the setting temperature. The time step of simulations is 1 fs. The initial temperature of substrates is 293 K. The models are relaxed for 800 ps using micro-canonical ensemble to reach equilibrium state. Then indenter vertically moves downward with velocity of 20 m/s. The maximum indentation depth is 3 nm. The embedded atom method potential<sup>[26]</sup> is used for the Cu–Cu, Al–Al, and Ag–Ag atom interactions. The C–C atom interaction is neglected as indenter is rigid body. Morse potential is employed for Al–C, Cu–C, and Ag–C atom interactions, where the cohesion energies are 0.28 eV, 0.087 eV, and 0.1 eV,

the size of substrates is much larger than the expected extent of plasticity zone, which is estimated to be up to 3.5 times the radius of indentation imprint in a worst-case scenario.<sup>[20,21]</sup> Hence, the size of our nanoindentation model is large enough to eliminate the size effect.

The GNT metallic multilayers, face-centered-cubic (FCC) single crystals, are structured by the twin layer with changed thicknesses of 3 nm, 5 nm, and 7 nm. The GNT Al, Cu, and Ag with the twin layer thickness of 3 nm, 5 nm, and 7 nm are defined as GNT Al-1, GNT Cu-1, and GNT Ag-1, respectively. In order to investigate the effect of gradient degree on the mechanical behavior, the GNT Al, Cu, and Ag with the twin layer thicknesses of 1 nm, 5 nm, and 9 nm are also constructed and named as GNT Al-2, GNT Cu-2, and GNT Ag-2, respectively.

the elastic moduli are  $2.78 \text{ \AA}^{-1}$ ,  $5.14 \text{ \AA}^{-1}$ , and  $1.7 \text{ \AA}^{-1}$ , and the atomic equilibrium distances are 2.2 Å, 2.05 Å, and 2.2 Å for Al, Cu, and Ag. The cut-off radius of Morse potential is 9.025 Å.<sup>[23]</sup>

The MD simulations are performed by LAMMPS.<sup>[24]</sup> OVITO is employed to visualize simulation data.<sup>[27]</sup> The common neighbor analysis (CNA) and dislocation extraction algorithm (DXA) are adopted to identify the atom feature and defect, where the grey means other atoms, the red represents HCP atoms, the blue expresses BCC atoms, the green suggests FCC atoms, and the lines in green regions indicate partial dislocations.<sup>[28,29]</sup>

## 3. Results and discussion

### 3.1. Model validation

In order to validate the validity of models, the SFEs of Ag, Cu and Al are calculated firstly by the current MD simulations, as shown in Fig. 2(a). The values are closed obviously to the experiment and simulation results,<sup>[30,31]</sup> which certifies the reliability of our simulation results. In addition, Fig. 2(b) gives the indentation force vs. indentation depth curves of the

GNT Ag-1, Cu-1, and Al-1. When the indentation depth is same, the indentation force decreases in turn for GNT Cu-1, Ag-1 and Al-1. In addition, the indentation forces of GNT Cu-1, Ag-1 and Al-1 are on an order of magnitude as those of the NT Al, Cu, and Ag at the same indentation depth which have been reported in the literature.<sup>[32]</sup> These results further demonstrate the validity of current simulations. It can be observed from Fig. 2(b) that the indentation force-depth curves fluctuate seriously during nanoindentation, indicating the complex microstructure evolution in the GNT metallic multilayers.<sup>[3,33]</sup> The lattice rearrangement and frequent dislocation interactions would induce the work hardening, and the dislocation nucleation and slip would cause the material softening.<sup>[34,35]</sup> The fluctuation of indentation force-depth curves and the corresponding evolution of microstructures are deeply discussed in the following sections.

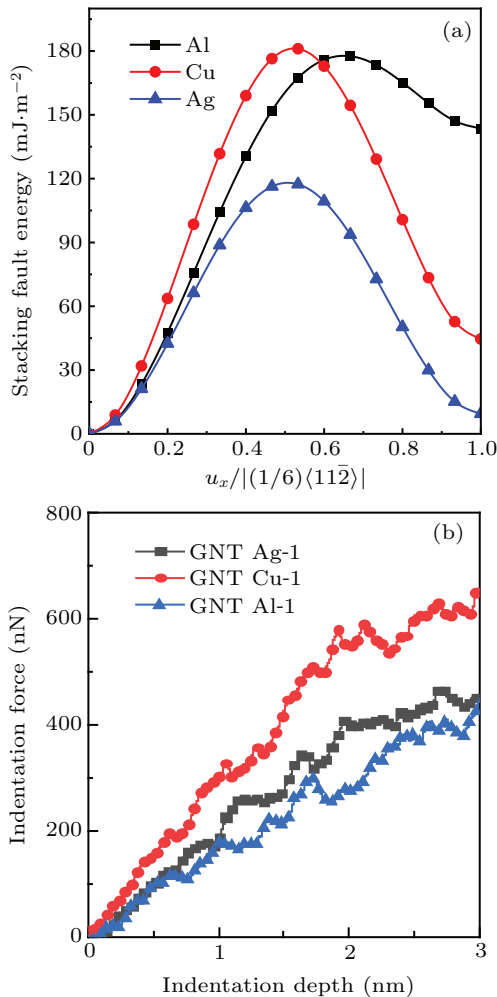


Fig. 2. Generalized stacking fault energies as a function of normalized Burgers vector in Ag, Cu, and Al (a). Indentation force vs indentation depth curves for GNT Ag-1, Cu-1, and Al-1 (b).

### 3.2. Deformation mechanism of GNT Ag

The mechanical responses and the plastic deformation mechanisms of GNT Ag, Cu, and Al are analyzed below. The plastic deformation of Ag often goes with a high amount

of SFs due to the low SFE of Ag.<sup>[36]</sup> Here, the plastic-deformation behavior of GNT Ag subjected to nanoindentation is analyzed in detail. The elastic deformation keeps on going from a in Fig. 3(a), until the dislocation emission at the indentation depth of 0.24 nm [b in Fig. 3(a)], as displayed in Fig. 3(b). Due to the dislocation intersection and blockage on TBs, the indentation force increases sustainably [b–c stage in Fig. 3(a)]. Then the indentation force decreases at c due to the TB migration [Fig. 3(c)], which is induced by the dislocation pile-up on TBs.<sup>[37]</sup> Since the strengthening effect of dislocation blockage on TBs is more prominent than the softening effect of TB migration and dislocation nucleation from TBs, the indentation force increases at the initiation of c–d stage. Subsequently, the indentation force mildly fluctuates in the elliptical region of c–d stage, indicating the competitive balance among the dislocation blockage on TBs, TB migration, and dislocation nucleation from TBs. The damaged part of TBs caused by the dislocation blockage, serves as the new dislocation nucleation site in TBs. The dislocation nucleation from TBs releases the local stress, leading to the decrease of indentation force. The phenomenon agrees well with the previous experiment result, which reports that the dislocation nucleation from TBs plays significant role in enhancing ductility of nanocrystal metals.<sup>[38]</sup>

It is noteworthy that the dislocation propagation parallel to the TB [marked by Disl. propagation in Fig. 3(e)] strengthens the GNT Ag, which contributes to the rise of indentation force-depth curve in the d–e stage. The dislocation propagation parallel to the TB is also observed in the nanoindentation experiment.<sup>[39]</sup> However, the curve drops in the e–f stage, due to the dislocation annihilation parallel to the TB, as marked Disl. annihilation in Fig. 3(f). With the indenter penetrating further, the dislocations blockage on the migrated TB [Disl. blockage in Fig. 3(g)], which leads to the increment of indentation force in the f–g stage. Interestingly, besides the dislocation blockage on TB, the dislocation propagation parallel to the TB is observed in Fig. 3(h). The dislocation propagation parallel to the TB exerts the strengthening effect by enhancing the resistance of dislocation motion. Subsequently, the GNT Ag is softened by further TB migration [Fig. 3(h)]. Thus, the hardening and softening cause the fluctuation of indentation force in the g–h stage. Compared with the Disl. propagation in Fig. 3(h), the corresponding dislocations annihilate afterward [Disl. annihilation in Fig. 3(i)], promoting the indentation force decrease in the h–i stage. To sum up, the dislocation propagation parallel to the TB and the corresponding dislocation annihilation, as well as the dislocation blockage on the TB, the TB migration and the dislocation nucleation from the TB dominate the plastic deformation of GNT Ag.

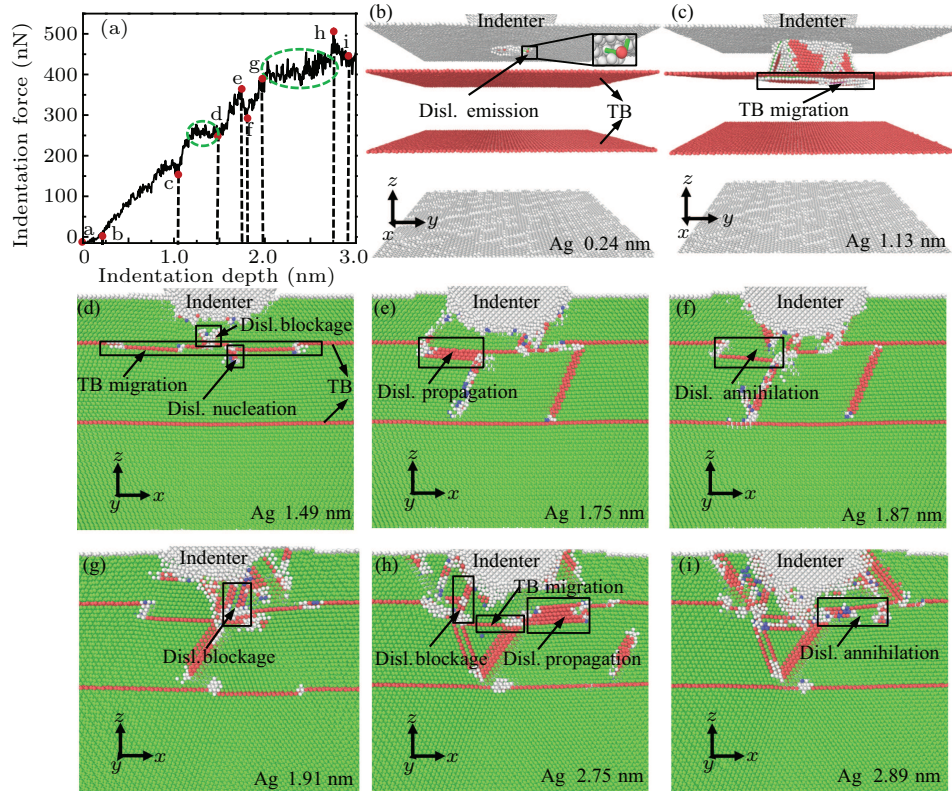


Fig. 3. Indentation force-depth curve of the GNT Ag (a). Microstructures of the GNT Ag at different indentation depths (b)–(i).

### 3.3. Deformation mechanism of GNT Cu

Figure 4(a) shows that the indentation force increases linearly with the indentation depth in the initial a–b stage, exhibiting the occurrence of elastic deformation in the GNT Cu. Subsequently, the dislocations nucleate and emit from the nanoindentation region [Fig. 4(b)]. The plastic deformation occurs and the indentation force decreases [b of Fig. 4(a)]. As the indenter penetrates, the hindrance of TB leads to the dislocation blockage on TB, causing the increase of indentation force in the b–c stage. As the dislocation blockage gets more serious, the TB migration occurs [Fig. 4(c)]. Hence, the indentation force decreases at the corresponding c in Fig. 4(a). In the following c–d stage, the plastic deformation of GNT Cu is mainly governed by the dislocation blockage, the TB migration and the dislocation nucleation from the TB [Fig. 4(d)], which agree well with the results reported by the previous nanoindentation experiment.<sup>[40]</sup> However, the indentation force increases in the c–d stage, indicating that compared with the TB migration and the dislocation nucleation from the TB, the dislocation blockage on TB is more dominant in this stage. The dislocation blockage on TB would lead to the material hardening. The TB migration and the dislocation nucleation from TB would soften the material. Figure 4(a) shows that the indentation force continues to increase in the d–e stage, which is ascribed to the combined contribution of twinning and dislocation propagation parallel to TB, as shown in Fig. 4(e). Both the twinning and the dislocation propagation

parallel to TB increase the motion resistance of other dislocations.

Compared with Fig. 4(e), the detwinning and dislocation annihilation appear afterward [Fig. 4(f)], which causes the reduction of indentation force in the e–f stage. It needs to be mentioned that the detwinning phenomenon is also found in the corresponding nanoindentation experiment.<sup>[41]</sup> It can be observed from Fig. 4(g) that the dislocation propagation parallel to TB, the dislocation blockage on TB, and the TB migration appear, which collectively dominate the fluctuation of indentation force in the f–g stage. The dislocation propagation parallel to TB enhances the resistance of dislocation motion, thereby strengthening the GNT Cu. The dislocation blockage on TB and the TB migration exert the strengthening and softening effects, respectively. Compared with Fig. 4(g), the dislocation annihilation occurs in Fig. 4(h), leading to the decrease of indentation force in the g–h stage. Figure 4(i) shows that the TB migration, the dislocation nucleation from TB, and the dislocation blockage on TB control the next plastic deformation. Obviously, the dislocation blockage on TB plays a prominent strengthening effect, resulting in the indentation force increase in the h–i stage. Besides the TB migration, the dislocation nucleation at TB, and the dislocation blockage on TB, the other dynamic behaviors including the twinning, the detwinning, the dislocation propagation parallel to TB, and the dislocation annihilation occur during the plastic deformation of GNT Cu.

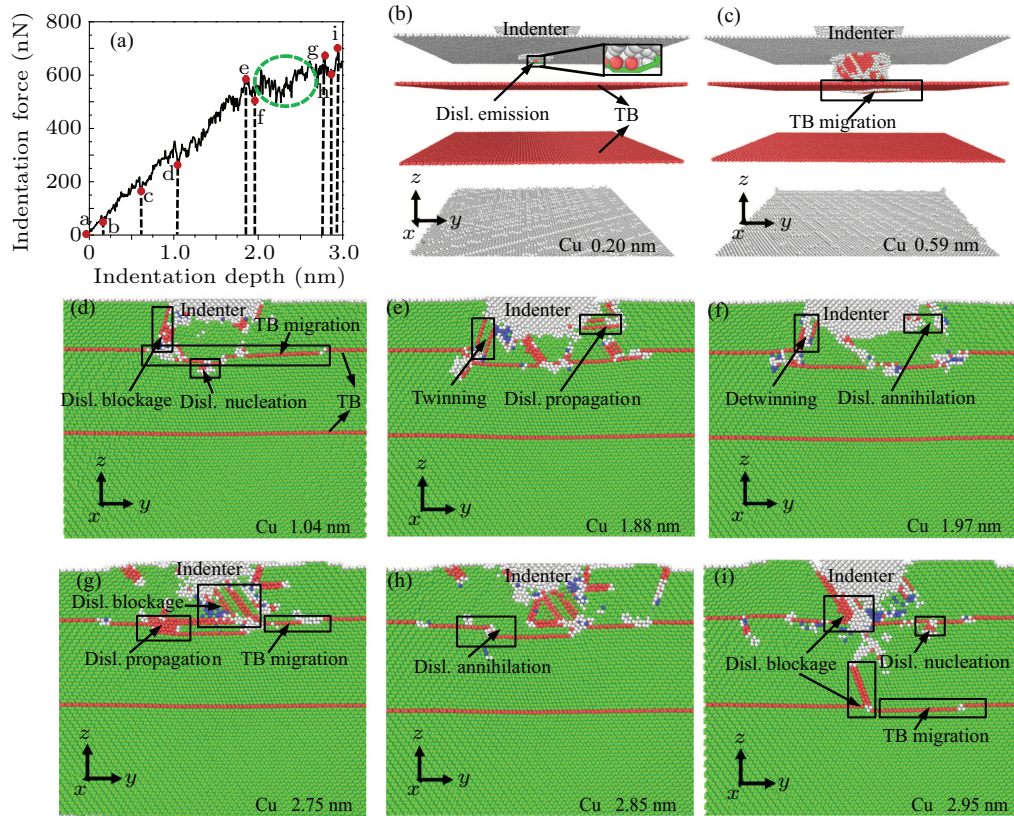


Fig. 4. Indentation force-depth curve of GNT Cu (a). Microstructures of GNT Cu at different indentation depths (b)–(i).

### 3.4. Deformation mechanism of GNT Al

The GNT Al firstly occurs with pure elastic deformation in the initial a–b stage in Fig. 5(a), at which the top surface pressed by indenter is sunk, but no internal defect is generated. When the indenter reaches indentation depth of 0.43 nm, the dislocations emit from the indentation region, see the marker dislocation (Disl.) emission in Fig. 5(b). As a result, the strain energy accumulated in the elastic stage is released, and the indentation force drops at b of Fig. 5(a). Subsequently, the motion of dislocations is hindered by TB, and the dislocations are restricted in the twin layer, which induces the work hardening. Therefore, the indentation force increases in the b–c stage of Fig. 5(a). Afterwards, the TB migration [Fig. 5(c)] leads to the decrease of indentation force at c of Fig. 5(a). Interestingly, the twinning occurs in the GNT Al [Fig. 5(d)]. The twinning would hinder the dislocation motion, thereby strengthen the material and cause the increment of indentation force in the c–d stage. In addition, it is observed that the indentation force-depth curve fluctuates in the d–e stage, due to the balanced competition between the strengthening and softening effects. The twinning and the dislocation blockage on the TB [Fig. 5(e)] both exert the strengthening effect. The TB migration [Fig. 5(e)] governs the softening effect in this stage.<sup>[35]</sup>

Additionally, the indentation force fluctuates in the e–f stage, which can be ascribed to the competitive balance among the detwinning, the TB migration, and the dislocation block-

age on the TB. Compared with Fig. 5(e), the detwinning occurs in Fig. 5(f), which is consistent with the result observed by the nanoindentation experiment.<sup>[41]</sup> In addition, the detwinning occurs at the indentation depth of 1.67 nm for the GNT Al and 1.97 nm for the GNT Cu [Figs. 4(f) and 5(f)]. The phenomenon reveals that the detwinning occurs earlier for the GNT Al than the GNT Cu, which was also reported in the previous nanoindentation experiment.<sup>[41]</sup> The detwinning will impair the motion resistance of dislocations and lead to the material softening. As indenter moves down, more dislocations emit under the indenter, which results in the serious dislocation blockage on TB, thereby causing the TB migration. It is observed in Fig. 5(a) that the indentation force-depth curve rises firstly in the f–g stage, indicating that the strengthening effect induced by the dislocation blockage on the TB is more prominent than the softening effect caused by the TB migration. Subsequently, the dislocation nucleation from the TB and the TB migration [Fig. 5(g)] together exert the softening effect, so the indentation force decreases in the second half of the f–g stage. The dislocations propagate from the upper TB downward and then pile up in the lower TB, resulting in the migration of lower TB [Fig. 5(h)]. The indentation force increases in the g–h stage, revealing that the dislocation blockage on the TB mainly governs the plastic deformation in this stage. Hereafter, the TB migration primarily controls the plastic deformation in the h–i stage [Fig. 5(i)], causing the decrease of indentation force with indentation depth. It is worth noting

that twinning and detwinning occur during the nanoindentation of GNT Al. The phenomena verify the previous theoretical report,<sup>[42]</sup> which proposed that the twin lamellae affects twinning and detwinning. The new phenomena of twinning

and detwinning the GNT Al are different from the nanoindentation response in the NT-Al, which is only dominated by the dislocation slip, the dislocation-TB interaction, and the TB migration.<sup>[30]</sup>

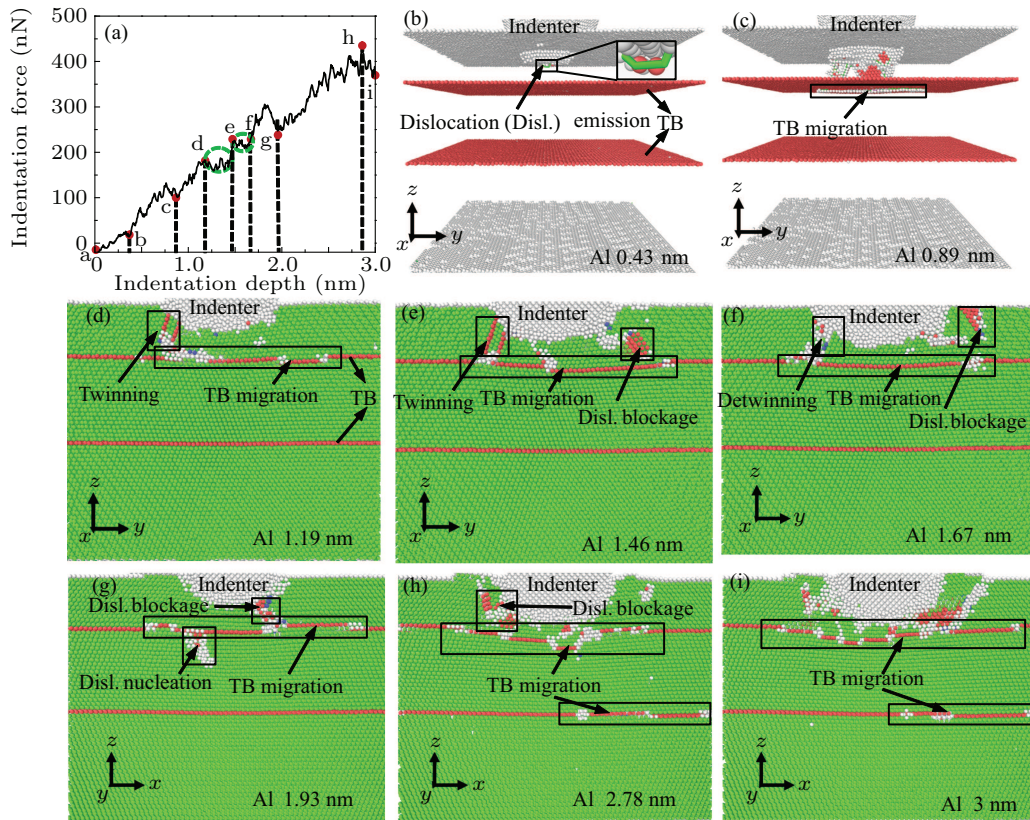


**Fig. 5.** Indentation force–depth curve of GNT Al (a), where some indentation steps are marked by red points. Microstructures of GNT Al at different indentation depths, described by DXA and CNA (b)–(i). In order to display defects, FCC atoms of green are hidden in (b) and (c), and the cross section views of substrate are exhibited in (d)–(i).

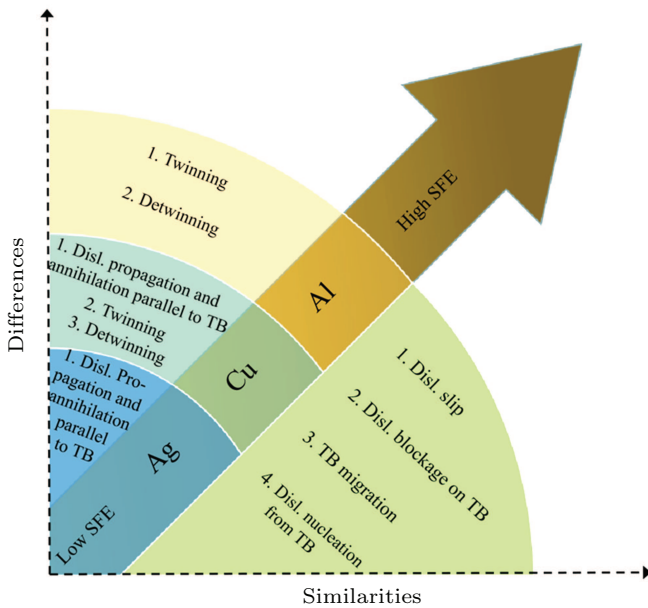


**Fig. 6.** Differences and similarities of the plastic-deformation behaviors in the GNT Ag, Cu, and Al subjected to nanoindentation.

To better understand the nanoindentation-induced plasticity in the GNT Ag, Cu, and Al, besides the dislocation slip, the dislocation blockage on the TB, the TB migration, and

the dislocation nucleation from the TB, several key events is schematically shown in Fig. 5. It is observed that during the nanoindentation, the dislocation slip, the dislocation blockage on the TB, the TB migration, and the dislocation nucleation from the TB occur in the plastic deformation process of the GNT Ag, Cu, Al. Differently, the deformation behavior transforms from the dislocation dynamics to the twinning/detwinning in the GNT Ag, Cu, to Al with the increasing SFE.

## 4. Effect of gradient degree

### 4.1. Strengthening effect on the GNT Ag

In order to reveal the effect of gradient degree on the mechanical behavior of the GNT Ag, The nanoindentation responses of GNT Ag-1 and GNT Ag-2 are contrasted and analyzed in detail. Figure 7(a) shows the indentation force–depth curves of GNT Ag-1 and GNT Ag-2. It can be seen that the indentation force of GNT Ag-2 is larger than that of GNT Ag-1 during the nanoindentation, indicating that a larger twin gradient strengthens the GNT Ag and improves its hardness. Figure 7(b) gives the evolution of dislocation line length dur-

ing the nanoindentation to explore the potential strengthening mechanism. Compared with GNT Ag-1, fewer dislocations are generated in GNT Ag-2 during the initial plastic stage, which manifests that the initial strengthening effect is dominated by the hindrance of the TB in GNT Ag-2. Subsequently, Fig. 7(b) exhibits a rapid increase in the length of dislocation line for GNT Ag-2 than GNT Ag-1. This rapid increase would lead to a sharp rise in the dislocation density, thereby causing significant work hardening and material strengthening. The above discussion suggests that the strengthening mechanism of GNT Ag-2 is the dislocation strengthening, as well as the TB strengthening. Therefore, a substantial strengthening effect can be achieved solely by increasing the twin gradient in GNT Ag.

To deeply understand the underlying strengthening mechanisms, we give the evolution of defects in GNT Ag-1 [Figs. 8(a)–8(d)] and GNT Ag-2 [Figs. 8(e)–8(h)] during the nanoindentation. At the initial of nanoindentation, the dislocations nucleate and propagate in GNT Ag-1 under the indenter [Fig. 8(a)], while these are restrained in GNT Ag-2 due to the hindering effect of the TB [Fig. 8(e)]. With the indentation depth increasing, the dislocations nucleate and emit from the upper TB into the lower TB of GNT Ag-2 [Fig. 8(f)]. In the meantime, the dislocations slip in the first twin layer of GNT Ag-1 [Fig. 8(b)]. In this stage, it is obvious that the strengthening effect from the upper TB plays an important role in GNT Ag-2, so a larger indentation force is required to reach same depth for the indenter. Subsequently, a large number of dislocations nucleate and extend downward from the upper TB to release severe stress concentration induced by strong hindrance effect of the TB in GNT Ag-2. As a result, compared

with the GNT Ag-1 [Figs. 8(c) and 8(d)], numerous dislocations exist in the second twin layer of GNT Ag-2 [Figs. 8(g) and 8(h)]. The dense dislocations increase the movement resistance of other dislocations, thereby strengthening the material and increasing the indentation force. The strengthening effect for GNT Ag-2 transforms from the TB strengthening to the dislocation strengthening with the indentation depth increasing.

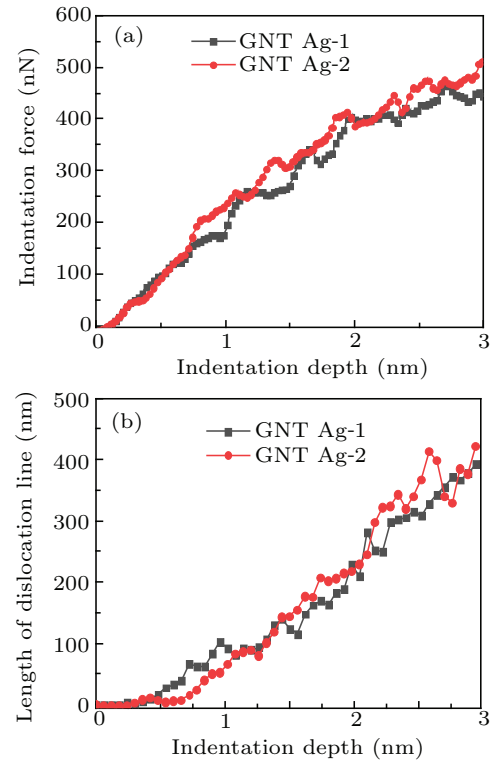


Fig. 7. Indentation force (a) and length of dislocation line (b) vs. indentation depth for GNT Ag-1 and GNT Ag-2.

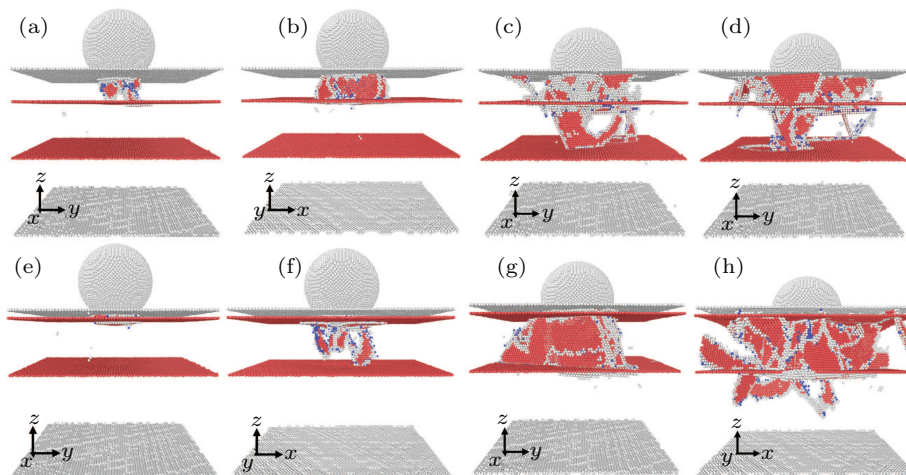


Fig. 8. Defect evolution of GNT Ag-1 (a)–(d) and GNT Ag-2 (e)–(h) with the increase of indentation depth 0.5 nm [(a), (e)], 1 nm [(b), (f)], 2.5 nm [(c), (g)], 3 nm [(d), (h)], where the atoms of FCC, BCC, HCP and other structures are colored in green, blue, red and white according to their CNA values, respectively. The atoms of FCC structure are hidden to clarify defects.

Figures 9(a) and 9(b) give the evolution of length of various dislocation lines and the number of atoms during the nanoindentation, respectively. It is found from Fig. 9(a) that lots of partial dislocations are produced by the nanoindentation

in GNT Ag-1 and GNT Ag-2, due to the low SFE of Ag. With the indentation depth increasing, the partial dislocations in GNT Ag-2, including the Shockley dislocations, frank dislocations, and stair-rod dislocations, are more than those

in GNT Ag-1. Correspondingly, more FCC atoms are transformed into the HCP atoms and other atoms, which constitute defect atoms in GNT Ag-2 [Fig. 9(b)]. These partial dislocations, especially stair-rod dislocations, cooperate with the defect atoms to block the dislocation motion and realize the dislocation strengthening.

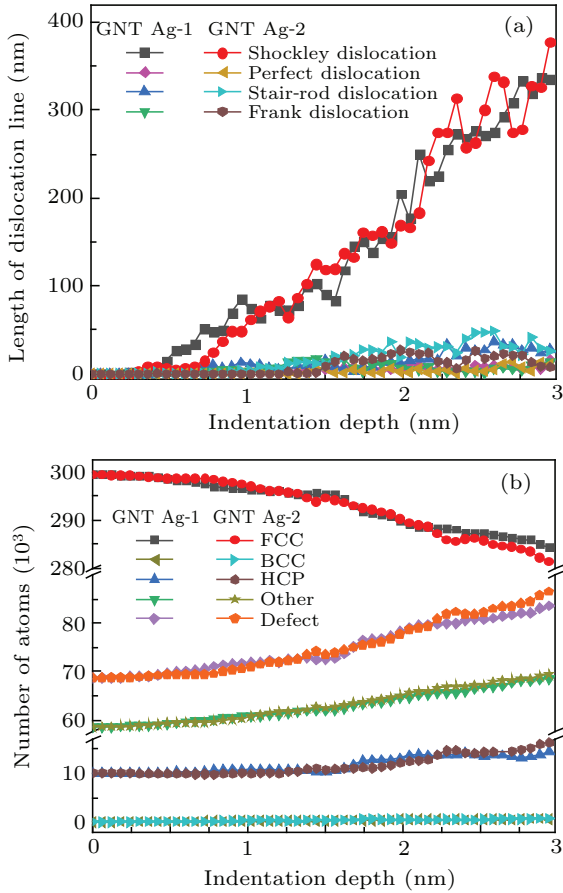


Fig. 9. Length of dislocation lines (a) and number of atoms (b) vs. indentation depth for GNT Ag-1 and GNT Ag-2.

#### 4.2. Strengthening effect on the GNT Cu

Figure 10(a) displays the indentation force vs. indentation depth curves of GNT Cu-1 and GNT Cu-2. A larger indentation force is needed for GNT Cu-2 than GNT Cu-1 at the same indentation depth, which is similar to GNT Ag-1 and GNT Ag-2. This phenomenon reveals that the GNT Cu can be strengthened by introducing a larger twin gradient. Figure 10(b) gives the evolution of dislocation line length during the nanoindentation to analyze the strengthening mechanism. When the indentation depth is less than 1.75 nm, fewer dislocations are produced in GNT Cu-2 than in GNT Cu-1 [Fig. 10(b)], while the indentation force is larger for GNT Cu-2 in this stage. This result indicates the TB strengthening by hindering the dislocation motion is main strengthening mechanism of GNT Cu-2 in the initial stage of nanoindentation. With the indentation depth increasing, the length of dislocation lines increases in GNT Cu-2 and GNT Cu-1. Interestingly, the dislocations increase faster in GNT Cu-2, which would cause that more dislocations pile

up in GNT Cu-2. A large amount of dislocation accumulation will increase the movement resistance of other dislocations, so as to realize the dislocation strengthening. As a result, the indenter requires a greater indentation force to reach the same indentation depth in GNT Cu-2 [Fig. 10(a)]. To sum up, the strengthening mechanism of GNT Cu-2 is the TB strengthening followed by the dislocation strengthening, which is the same as that of GNT Ag-2. This result indicates that the GNT Cu can also be strengthened by increasing the twin gradient.

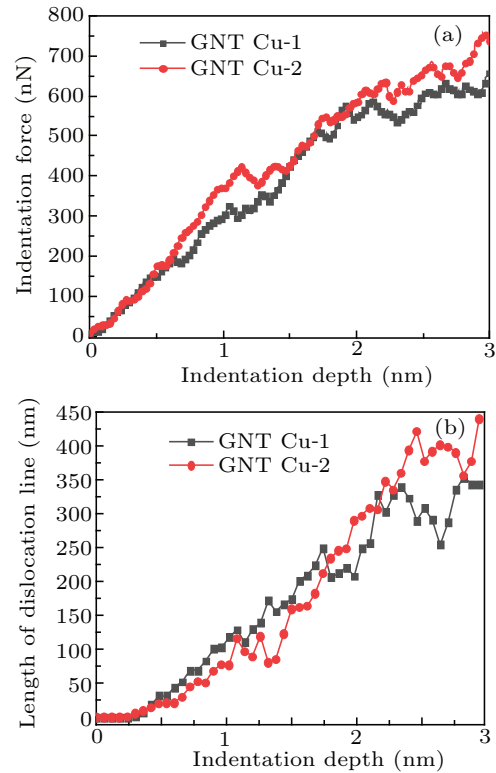


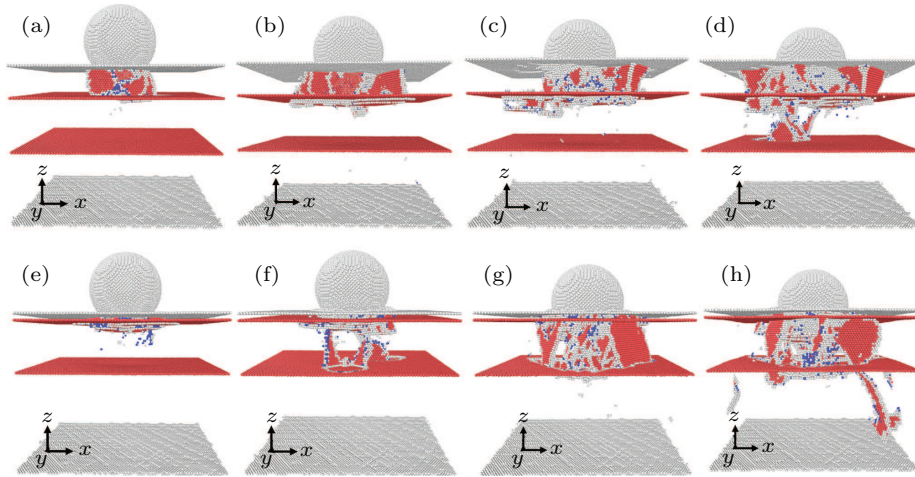
Fig. 10. Indentation force (a) and length of dislocation lines (b) vs. indentation depth for GNT Cu-1 and GNT Cu-2.

Figure 11 exhibits the detailed process of defect evolution during the nanoindentation of GNT Cu-1 and GNT Cu-2, to give an insight into the strengthening mechanism. It can be seen that, when the dislocations nucleate and extend within the first twin layer of GNT Cu-1 [Fig. 11(a)], the dislocation motion is effectively suppressed by the upper TB in GNT Cu-2 and the TB migration occurs to release the stress concentration [Fig. 11(e)]. Subsequently, some dislocations nucleate and emit from the upper TB into the second twin layer, and then pile up on the lower TB due to the hindering effect of this TB [Fig. 11(f)]. However, the dislocations keep extend within the first twin layer of GNT Cu-1, owing to larger thickness of twin layer [Fig. 11(b)]. Hence, it is the hindering effect of the TB that the indentation force is larger for GNT Cu-2 than GNT Cu-1. The TB strengthening is main strengthening mechanism at this initial stage of nanoindentation for GNT Cu-2. As the indentation depth increases, more dislocations nucleate from the upper TB, and then extend extensively within the second twin layer with large thickness to release severe stress

concentration induced by first twin layer with small thickness [Figs. 11(g) and 11(h)]. Consequently, numerous dislocations exist in GNT Cu-2, causing the dislocation strengthening.

In addition, Figs. 12(a) and 12(b) show the evolution of the length of various dislocations lines and the number of atoms in GNT Cu-1 and GNT Cu-2 during the nanoindentation. It can be seen from Fig. 12(a) that the nanoindentation mainly induces partial dislocations, including Shockley dislocations, stair-rod dislocations, and frank dislocations to nucleate and propagate in GNT Cu-1 and GNT Cu-2. Correspondingly, the FCC atoms are turned into the defect atoms

which consist of the HCP atoms and other atoms [Fig. 12(b)]. As the indentation depth increases, the Shockley dislocations increase greatly. When the indentation depth is larger than 1.75 nm, the stair-rod dislocations besides the Shockley dislocations increase more significantly in GNT Cu-2 than in GNT Cu-1 and more defect atoms are generated, which bring about the dislocation strengthening. To sum up, the GNT Ag and the GNT Cu can be strengthened by increasing the twin gradient, where the TB strengthening and the dislocation strengthening are mainly strengthening mechanism.



**Fig. 11.** Defect evolution of GNT Cu-1 (a)–(d) and GNT Cu-2 (e)–(h) for indentation depths 1 nm [(a), (e)], 1.5 nm [(b), (f)], 2.5 nm [(c), (g)], and 3 nm [(d), (h)], where the atoms of FCC, BCC, HCP and other structures are colored in green, blue, red and white according to their CNA values, respectively. The atoms of FCC structure are hidden to clarify defects.

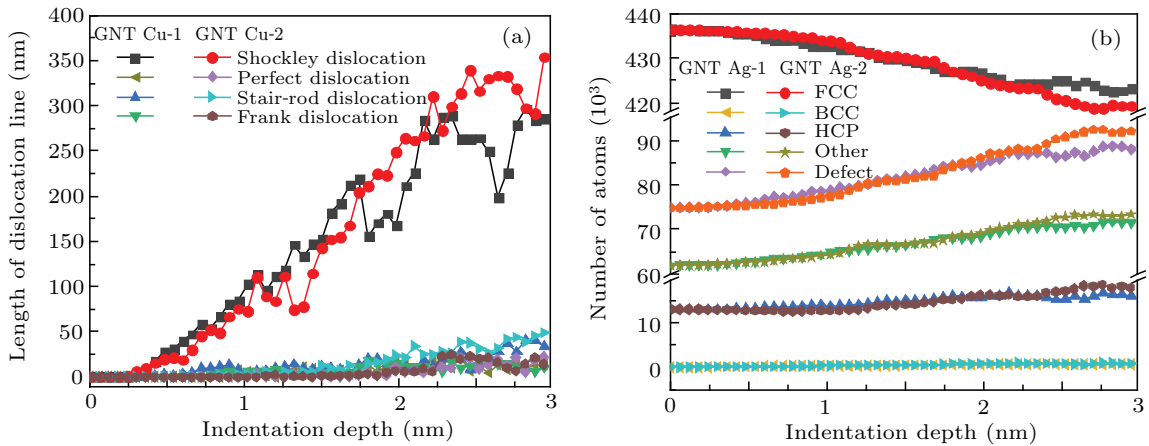


**Fig. 12.** Length of dislocation lines (a) and number of atoms (b) vs. indentation depth for GNT Cu-1 and GNT Cu-2.

### 4.3. Softening effect on the GNT Al

Figure 13(a) gives the indentation forcedepth curves of GNT Al-1 and GNT Al-2. At the initial of nanoindentation, the indentation force in GNT Al-2 is smaller than that in GNT Al-1. In the meanwhile, the lengths of dislocation lines for both GNT Al-1 and GNT Al-2 are almost the same in this stage [Fig. 13(b)]. As the indenter penetrates, although the indentation force acting on the GNT Al-2 is greater, it soon becomes smaller than that exerting on GNT Al-1 [Fig. 13(a)]. However,

the length of dislocation lines in GNT Al-2 is almost always smaller than that in GNT Al-1, except that there occurs a sudden drop at the end of nanoindentation [Fig. 13(b)]. Therefore, it can be concluded that GNT Al-2 is mainly softened by a larger twin gradient during the whole nanoindentation stage, which is obviously different from GNT Ag-2 and GNT Cu-2. The evolution of the indentation force and the dislocation line length with the indentation depth, and the softening mechanism are analyzed in detail below.

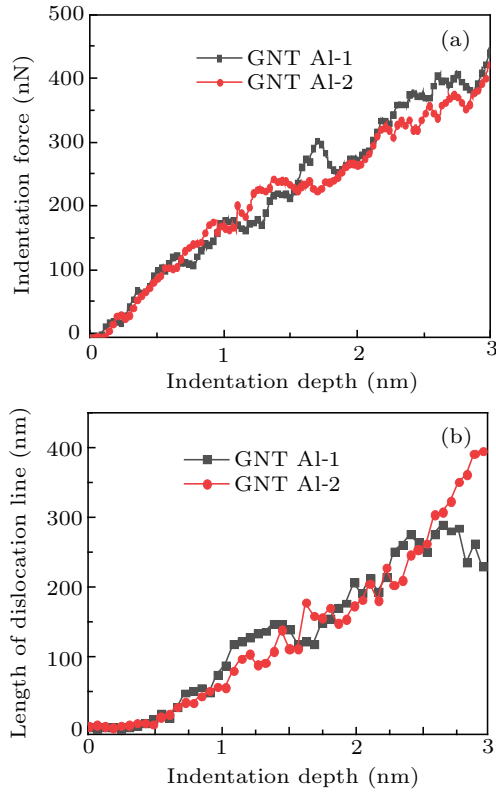


**Fig. 13.** Indentation force (a) and length of dislocation lines (b) vs. indentation depth for GNT Al-1 and GNT Al-2.

The defects in GNT Al-1 and GNT Al-2 induced by the nanoindentation are exhibited in Fig. 14. It can be observed from Fig. 14(a) that there is almost no the TB migration in GNT Al-2 in the initial stage of nanoindentation, and the dislocations directly nucleate and emit from the upper TB into the second twin layer. This is because the stress required to the TB migration in GNT Al-2 is very high,<sup>[4]</sup> as compared to

that in GNT Cu-2 and GNT Ag-2. The dislocation nucleation and emission from the upper TB would lead to the material softening, which has been reported theoretically in the previous study.<sup>[35]</sup> Hence, the indentation force is smaller in GNT Al-2 than in GNT Al-1 in this initial stage [Fig. 13(a)]. Subsequently, the dislocations extend to the lower TB instead of slipping within the second twin layer of GNT Al-2 due to the high SFE of Al. Soon after, the dislocation motion is impeded by the second TB [Fig. 14(f)], so a larger indentation force is required for GNT Al-2 in this stage [Fig. 13].

However, with the indentation depth increasing, GNT Al-2 is softened as more dislocations nucleate and emit from the upper TB into the lower TB [Fig. 14(g)]. In the meantime, many dislocations are emitted from the indentation region of GNT Al-1, and mainly pile up on the upper TB, as shown in Fig. 14(c). The massive dislocation accumulation leads to the strengthening of GNT Al-1. As the indenter continues to move down, more dislocations are induced in the indentation region of GNT Al-1 [Fig. 14(c)], enhancing the dislocation strengthening effect. For GNT Al-2, the dislocation density in the second twin layer also increases due to the more dislocation nucleation and emission from the upper TB. As a result, the dense dislocations accumulate on the lower TB, leading to high stress concentration in this TB. When the stress reaches the critical stress of TB migration, the TB migrates [Fig. 14(h)] and GNT Al-2 is softened. To sum up, a larger twin gradient causes the softening of GNT Al, which is different from the GNT Ag and the GNY Cu. The dislocation nucleation from the TB and the TB migration are the main softening mechanism of GNT Al-2.

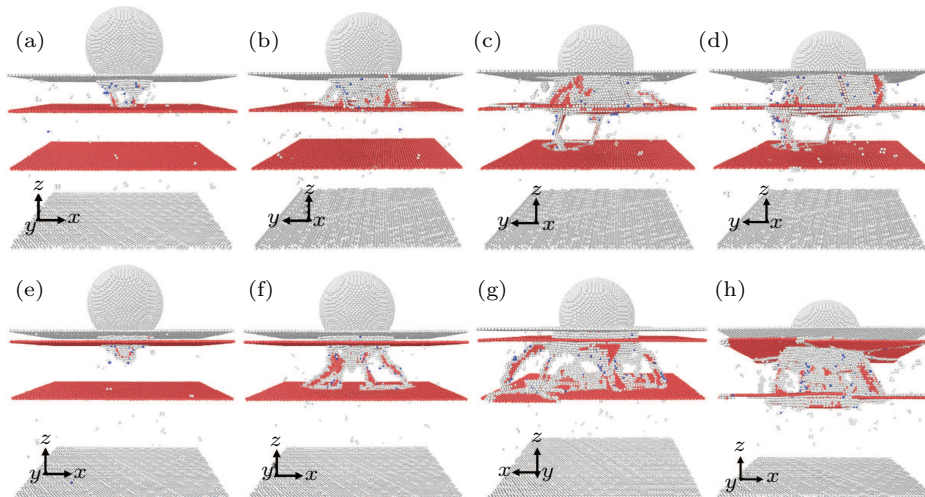


**Fig. 14.** Defect evolution of GNT Al-1 (a)–(d) and GNT Al-2 (e)–(h) for indentation depths 0.5 nm [(a), (e)], 1.2 nm [(b), (f)], 2.5 nm [(c), (g)], and 3 nm [(d), (h)], where the atoms of FCC, BCC, HCP, and other structures are colored in green, blue, red and white according to their CNA values, respectively. The atoms of FCC structure are hidden to clarify defects.

To take a closer look at the defect evolution, the length of various dislocation lines and the number of atoms vs. the indentation depth in the GNT Al-1 and GNT Al-2 are given in Figs. 15(h) and 15(b), respectively. It can be seen from

Fig. 15(h) that the nanoindentation mainly induces the Shockley dislocations generated in GNT Al-1 and GNT Al-2 in the initial stage, and the lengths of Shockley dislocations in both of them are almost the same. The stair-rod dislocations are

additionally produced in GNT Al-1, increasing the motion resistance of other dislocations and the capacity of work hardening. Afterwards the obviously less Shockley dislocations are generated in GNT Al-2 than in GNT Al-1 [Fig. 15(h)], accompanied by the fact that fewer FCC atoms are converted to the defect atoms [Fig. 15(b)]. The result is attributed to the hindering effect of the TB described in Fig. 14.

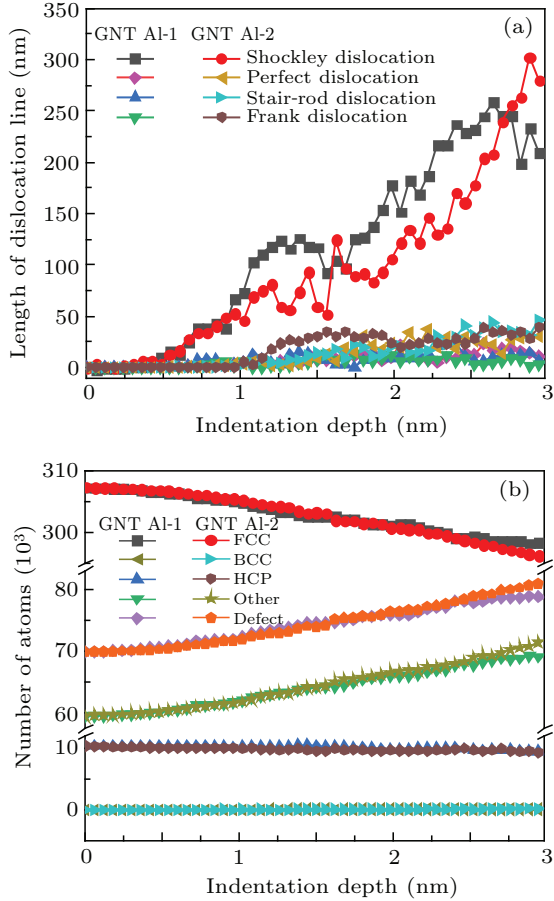


**Fig. 15.** Length of dislocation lines (a) and number of atoms (b) vs. indentation depth for GNT Al-1 and GNT Al-2.

As the indentation depth increases, the numbers of HCP atoms and BCC atoms almost keep constant while other atoms increase obviously. This phenomenon demonstrates that the nanoindentation induces the transition of the FCC atoms in GNT Al-1 and GNT Al-2 to the defect atoms, mainly other atoms rather than HCP atoms, which is attributed to the high SFE of Al. Compared with GNT Al-1, the defect atoms are more in GNT Al-2 [Fig. 15(b)]. Furthermore, the Shockley dislocations in GNT Al-2 sharply increase, while more perfect dislocations, stair-rod dislocations and frank dislocations are induced in GNT Al-2 than in GNT Al-1 [Fig. 15(a)], which exacerbates the dislocation pile-up on TB. Consequently, the TB migration occurs and GNT Al-2 is softened.

## 5. Theoretical analysis

The above discussions reveal that the GNT Ag and GNT Cu can be strengthened by increasing the twin gradient. The

TB strengthening and the dislocation strengthening are mainly the strengthening mechanism. However, the GNT Al softens when the twin gradient is increased. The defect analysis have demonstrated that the dislocation nucleation from the TB and the TB migration are mainly softening mechanism. In order to further quantitatively investigate the softening effect of large twin gradient on the GNT Al, the theoretical model is built.

The total strain rate consisting of elastic strain rate and plastic strain rate can be expressed as

$$\dot{\epsilon} = \dot{\epsilon}_e + \dot{\epsilon}_p. \quad (1)$$

The elastic strain rate follows Hooke's law  $\dot{\epsilon}_e = \mathbf{M} : \dot{\boldsymbol{\sigma}}$ . The plastic strain can be expressed as

$$\dot{\epsilon}_p = \frac{3}{2} \frac{\dot{\epsilon}_p}{\sigma} \boldsymbol{\sigma}', \quad (2)$$

where  $\dot{\epsilon} = \sqrt{2\dot{\epsilon}_{p_{ij}}\dot{\epsilon}_{p_{ij}}/3}$  denotes the Von Mises equivalent plastic strain rate,  $\sigma = \sqrt{3\sigma'_{ij}\sigma'_{ij}/2}$  represents the Von Mises equivalent stress, and 1 is the deviatoric stress tensor. The relationship between the equivalent plastic strain rate and equivalent stress is

$$\dot{\epsilon}_p = \dot{\epsilon} \left( \frac{\sigma}{\sigma_{\text{flow}}} \right)^m, \quad (3)$$

where  $\dot{\epsilon} = \sqrt{2\dot{\epsilon}'_{ij}\dot{\epsilon}'_{ij}/3}$  represents the equivalent strain rate;  $m$  is the sensitivity coefficient of rate;  $\sigma_{\text{flow}}$  is the flow stress, which depends on the specific microstructure.

In the present work, for the GNT Al, the contribution of TBs to the flow stress depends on the twin thickness.<sup>[43]</sup> The twin strengthening can be calculated by

$$\sigma_{\text{twin}} = M \sum_{\lambda} f_{\lambda} \left( \tau_l + \alpha \mu \frac{\pi}{8} \frac{2-v}{1-v} \frac{\lambda}{d} e^T + \varphi \frac{\gamma_{\text{tb}}}{\lambda e^T} \right), \quad \lambda \leq \lambda_c, \quad (4a)$$

$$\sigma_{\text{twin}} = M \sum_{\lambda} f_{\lambda} \frac{1}{n} \left( \frac{\gamma_{\text{sf}}}{b^p} + \frac{\mu b}{3\lambda} \right), \quad \lambda > \lambda_c, \quad (4b)$$

where  $M$  is the Taylor factor,  $f_{\lambda}$  denotes the volume fraction for twins with the twin thickness of  $\lambda$ ;  $\tau_l$  is the lattice resistance of TB migration;  $\alpha$  is a coefficient on the order of unit;  $\mu$  and  $\nu$  are the shear modulus and the Poisson's ratio, respectively;  $d$  is the grain size,  $e^T$  represents the transformation shear strain,  $\varphi$  is a constant denoting the formation of a TB;  $\gamma_{\text{tb}}$  and  $\gamma_{\text{sf}}$  are the energy of a TB and SFE, respectively;  $n$  denotes the geometrical parameter;  $b^p$  and  $b$  are the Burger vectors of partial dislocation and perfect dislocation. By comparing the calculation results of Eqs. (4a) and (4b) (see Fig. 16), the TB strength has a maximum value when the twin thickness is the critical value of  $\lambda_c$ . Equation (4a) is applicable to the twin thickness below the critical thickness, and Eq. (4b) is used when the twin thickness is larger than the critical thickness.

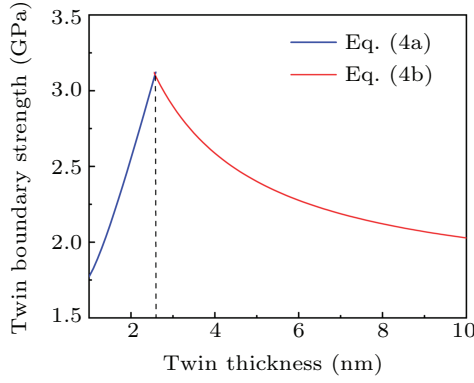


Fig. 16. Determination of critical twin thickness.

In addition, the dislocation is an important deformation mechanism, and its contribution to strength can be expressed as<sup>[44,45]</sup>

$$\sigma_d = M\beta\mu b\sqrt{\rho}, \quad (5)$$

where  $\beta$  is Taylor constant, and  $\rho$  is the dislocation density. Considering the dislocation propagation and annihilation inside grain, the evolution of dislocation density can be written as

$$\frac{d\rho}{d\varepsilon_p} = M \left( \frac{1}{bd} + \frac{\psi}{b} \sqrt{\rho} - k_{20} \left( \frac{\dot{\varepsilon}_p}{\dot{\varepsilon}_0} \right)^{-\frac{1}{n_0}} \rho - \left( \frac{d_e}{d} \right)^2 \rho \right), \quad (6)$$

where  $\psi$  is the proportionality factor,  $k_{20}$  is the dynamic annihilation constant-independent of size,  $\dot{\varepsilon}_0$  is the reference strain rate, and  $n_0$  is the dynamic recovery constant;  $d_e$  is the critical grain size when the dislocation annihilation occurs violently.

From the above analysis, the flow stress can be expressed as

$$\sigma_{\text{flow}} = \sigma_0 + \sigma_{\text{twin}} + \sigma_d, \quad (7)$$

where  $\sigma_0$  is the lattice resistance, whose value is 100 MPa for the metal of Al. All the parameters are list in Table 1.

Base on the above deduction and calculation, the contributions of each mechanism to the strength are shown in Fig. 17. In the GNT Al, the contribution of each mechanism to the flow stress is different. The blue line represents the contributions of dislocation and lattice to the total strength, which are feeble. The red line denotes the contribution of TB, which is significantly larger than those of dislocation and lattice. Comparing Figs. 17(a) and 17(b), it is found that the contribution of the TB to the yield stress is about 2.4 GPa for GNT Al-1, and it is about 1.9 GPa for GNT Al-2. The stress contributed by TB is obviously smaller in the GNT Al-2 than in GNT Al-1, which is the primary reason for the smaller total stress in GNT Al-2 (comparing the black lines in Figs. 17(a) and 17(b)). This result further demonstrates that the increase of twin gradient causes the GNT Al-2 to be softer than GNT Al-1 in the current study.

Table 1. Constitutive parameters of the GNT Al.<sup>[43–45]</sup>

Parameter	Symbol	Magnitude
Grain size (nm)	$d$	20
Shear modulus (GPa)	$\mu$	26
Poisson's ratio	$\nu$	0.3
Burger vector (nm)	$b$	0.258
Taylor factor	$M$	3.06
Coefficient	$\alpha$	0.4
Coefficient	$\varphi$	2
Twin stacking fault energy (mJ/m <sup>2</sup> )	$\gamma_b$	70
Stacking fault energy (mJ/m <sup>2</sup> )	$\gamma_f$	148
Burgers vector of partial dislocation (nm)	$b^p$	0.149
Taylor constant	$\beta$	0.3
Transformation shear strain	$e^T$	0.707
Dynamic recovery constant	$n$	21.5
Proportionality factor	$\psi$	0.025
Dynamic recovery constant	$K_{20}$	21
The critical grain size (nm)	$d_e$	580
Reference strain rate (s <sup>-1</sup> )	$\dot{\varepsilon}_0$	1

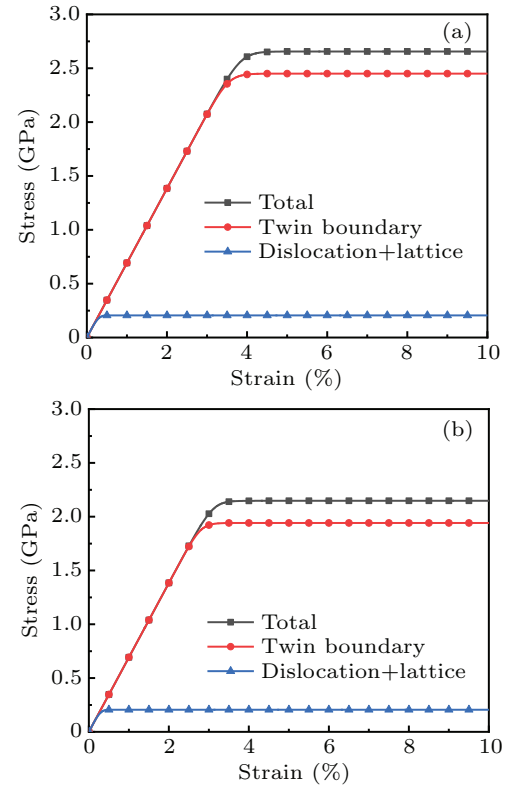


Fig. 17. Stress-strain response contributed by different mechanisms for GNT Al-1 (a) and GNT Al-2 (b).

## 6. Conclusions

Nanoindentations on GNT Ag, Cu, and Al are performed by MD simulations to explore the plastic-deformation behaviors of the GNT metallic multilayers with different SFEs from atomic level. The results shows that the dislocation blockage on TB, the TB migration, the dislocation nucleation from TBs always occur during the plastic deformation of GNT Al, Cu, and Ag. Additionally, the twinning and detwinning appear during the plastic deformation of GNT Al. The deformation behavior transforms from the dislocation dynamics to the twin-

ning/detwinning in GNT Ag, Cu, to Al with the increasing SFE.

In addition, it is uncovered that GNT Ag and GNT Cu strengthen at larger twin gradient due to more significant TB strengthening and dislocation strengthening. However, the GNT Al softens due to severer TB migration and dislocation nucleation from the TB in the case of larger twin gradient. The softening mechanism is further analyzed theoretically. These results not only promote a deeper understanding of the plastic-deformation behaviors of certain GNT metallic multilayers with different SFEs, but also provide a reference for the design of GNT metallic multilayers with required mechanical properties.

## Acknowledgements

The authors would like to deeply appreciate the support from the Foundation for Innovative Research Groups of the National Natural Science Foundation of China (Grant Nos. 51621004, 11572118, 51871092, and 11772122) and the National Key Research and Development Program of China (Grant No. 2016YFB0700300).

## References

- [1] Han Z, Liu H, Li Q, Zhou D and Lv J 2021 *Chin. Phys. Lett.* **38** 046201
- [2] Shao Y F, Meng F S, Li J H and Zhao X 2019 *Acta Phys. Sin.* **68** 216201 (in Chinese)
- [3] Wang J and Huang H 2006 *Appl. Phys. Lett.* **88** 203112
- [4] Bufford D, Liu Y, Wang J, Wang H and Zhang X 2014 *Nat. Commun.* **5** 4864
- [5] Huang C, Peng X H, Yang B, Zhao Y B, Xiang H G, Chen X, Li Q B and Fu T 2017 *Ceram. Int.* **43** 16888
- [6] Thevamaran R, Lawal O, Yazdi S, Jeon S J, Lee J H and Thomas E L 2016 *Science* **354** 312
- [7] Wei Y J, Li Y Q, Zhu L C, Liu Y, Lei X Q, Wang G, Wu Y X, Mi Z L, Liu J B, Wang H T and Gao H J 2014 *Nat. Commun.* **5** 3580
- [8] Zhang J J, Wang Z F, Sun T and Yan Y D 2016 *Mater. Res. Express* **3** 125018
- [9] Xiao Q X, Hou Z Y, Li C and Niu Y 2021 *Chin. Phys. B* **30** 056101
- [10] Zhu Y X, Li Z H, Huang M S and Liu Y 2015 *Int. J. Plast.* **72** 168
- [11] Huang C, Peng X, Fu T, Chen X, Xiang H, Li Q and Hu N 2017 *Mater. Sci. Eng. A* **700** 609
- [12] Liu P, Xie J, Wang A, Ma D and Mao Z 2020 *Mater. Chem. Phys.* **252** 123263
- [13] Tadmor E B and Bernstein N 2004 *J. Mech. Phys. Solids* **52** 2507
- [14] English A T and Chin G Y 1965 *Acta Metall.* **13** 1013
- [15] Feng Q, Song X, Xie H, Wang H, Liu X and Yin F 2017 *Mater. Design* **120** 193
- [16] Fu T, Peng X, Chen X, Weng S, Hu N, Li Q and Wang Z 2016 *Sci. Rep.* **6** 35665
- [17] Yang B, Zheng B, Hu X, Zhang K, Li Y, He P and Yue Z 2016 *Comput. Mater. Sci.* **114** 172
- [18] Alhafez I A, Ruestes C J, Gao Y and Urbassek H M 2015 *Nanotechnology* **27** 045706
- [19] Imran M, Hussain F, Rashid M and Ahmad S A 2012 *Chin. Phys. B* **21** 116201
- [20] Durst K, Backes B and Göken M 2005 *Scripta Mater.* **52** 1093
- [21] Durst K, Backes B, Franke O and Göken M 2006 *Acta Mater.* **54** 2547
- [22] Su M J, Deng Q, Liu L T, Chen L Y, Su M L and An M R 2021 *Chin. Phys. B* **30** 096201
- [23] Tian Y Y, Li J, Hu Z Y, Wang Z P and Fang Q H 2017 *Chin. Phys. B* **26** 126802
- [24] Stadler J, Mikulla R and Trebin H R 1997 *Int. J. Mod. Phys. C* **8** 1131
- [25] Li J, Fang Q, Liu B, Liu Y and Liu Y 2016 *J. Micromech. Mol. Phys.* **1** 1650001
- [26] Daw M S, Foiles S M and Baskes M I 1993 *Mater. Sci. Rep.* **9** 251
- [27] Stukowski A 2009 *Model. Simul. Mater. Sci.* **18** 015012
- [28] Su M J, Deng Q, An M R and Liu L T 2020 *Chin. Phys. B* **29** 116201
- [29] Zepeda-Ruiz L A, Stukowski A and Opperstrup T 2017 *Nature* **550** 492
- [30] Tadmor E B, Bernstein N 2004 *J. Mech. Phys. Solids* **52** 2507
- [31] English A T and Chin G Y 1965 *Acta Metall.* **13** 1013
- [32] Kulkarni Y and Asaro R J 2009 *Acta Mater.* **57** 4835
- [33] Wang J, Zhou Q, Shao S and Misra A 2017 *Mater. Res. Lett.* **5** 1
- [34] Alhafez I A, Ruestes C J, Bringa E M and Urbassek H M 2019 *J. Mech. Phys. Sol.* **132** 103674
- [35] Li X Y, Wei Y J, Lu L, Lu K and Gao H J 2010 *Nature* **464** 877
- [36] Liu L, Shen D, Zou G, Peng P and Zhou Y 2016 *Scripta Mater.* **114** 112
- [37] Fang Q H and Zhang L C 2016 *J. Micromech. Mol. Phys.* **01(02)** 1650008
- [38] Lu L, Zhu T, Shen Y, Dao M, Lu K and Suresh S 2009 *Acta Mater.* **57** 5165
- [39] Bufford D, Wang H and Zhang X 2011 *Acta Mater.* **59** 93
- [40] Li N, Wang J, Misra A, Zhang X, Huang J Y and Hirth J P 2011 *Acta Mater.* **59** 5989
- [41] Wang J, Li N, Anderoglu O, Zhang X, Misra A, Huang J Y and Hirth J P 2010 *Acta Mater.* **58** 2262
- [42] Zhu T and Gao H J 2012 *Scripta Mater.* **66** 843
- [43] Wei Y 2011 *Phys. Rev. B* **83** 132104
- [44] Li J and Soh A K 2012 *Int. J. Plasticity* **39** 88
- [45] Li J, Li L, Jiang C, Fang Q, Liu F, Liu Y and Liaw P K 2020 *J. Mater. Sci. Technol.* **57** 85